

Oxidation of Organosolv Lignin in a Novel Surfactant-free Microemulsion Reactor

Juanhua Kong¹, Lixia Li¹, Xin Luo¹, Qiang Zeng¹, Xiumin Chen¹, Zhenping Cai¹, Jinxing Long¹, Sijie Liu¹, Xuehui Li¹, Hongyan He², and Yingying Wang¹

¹South China University of Technology

²Institute of Process Engineering Chinese Academy of Sciences

May 22, 2020

Abstract

Lignin is considered as a promising substitute for fossil resources, but the efficient conversion of the lignin remains a huge challenge due to its structural complexity and immiscibility with typical solvents. Herein, a series of surfactant-free microemulsion reactors comprised of octane, water and n-propanol were designed and their corresponding phase behaviors alongside their ability to intensify oxidative depolymerization of lignin was explored. Experimental results show that the phenolic monomer yield improves substantially (40-500 wt.%) when the novel microemulsion systems are employed by comparison with processes performed in a single solvent. Detailed characterizations also suggest that the above intensification is rationalized by the solubilization effect of the microemulsion system, which arise as a consequence of directional aggregation of lignin at the microemulsion interface.

Oxidation of Organosolv Lignin in a Novel Surfactant-free Microemulsion Reactor

Juanhua Kong, Lixia Li, Xin Luo, Qiang Zeng, Xiumin Chen, Zhenping Cai, Jinxing Long, Sijie Liu* and Xuehui Li*

School of Chemistry and Chemical Engineering, State Key Laboratory of Pulp and Paper Engineering, South China University of Technology, Guangzhou, 510640, China.

Hongyan He

Beijing Key Laboratory of Ionic Liquids Clean Process, Institute of Process Engineering, Chinese Academy of Sciences, Beijing, 100190, China.

Yingying Wang

South China Advanced Institute for Soft Matter Science and Technology, South China University of Technology, Guangzhou, 510640, China.

Lignin is considered as a promising substitute for fossil resources, but the efficient conversion of the lignin remains a huge challenge due to its structural complexity and immiscibility with typical solvents. Herein, a series of surfactant-free microemulsion reactors comprised of octane, water and n-propanol were designed and their corresponding phase behaviors alongside their ability to intensify oxidative depolymerization of lignin was explored. Experimental results show that the phenolic monomer yield improves substantially (40-500 wt.%) when the novel microemulsion systems are employed by comparison with processes performed in a single solvent. Detailed characterizations also suggest that the above intensification is rationalized by the solubilization effect of the microemulsion system, which arise as a consequence of directional aggregation of lignin at the microemulsion interface.

Keywords: surfactant-free microemulsion, phase behavior, lignin oxidation, process intensification, metal sulfate

Introduction

Biomass is the most abundant renewable resources on earth, and is considered to be a promising substitute for fossil resources due to its vast concentration of carbon and hydrogen.¹ As the second largest component of biomass, lignin is presently underutilized due to its structural complexity, poor solubility and high bond dissociation energy.² Conversely, cellulose and hemicellulose are used widely for the production of bio-ethanol and sugars industrially.³ At present, 50-70 million tons of lignin is produced annually from pulping activities, but only ~2% of it is commercially utilized as value-added materials, such as water-reducing admixtures or as a surfactant, *etc*.⁴ On the other hand, it is regarded as the only renewable source of key- and high-volume aromatic polymers, making it a potential green precursor for the production of aromatic products usually refined from petroleum.^{5,6} Therefore, the development of efficient technologies for the production of value-added chemicals *via* lignin depolymerization is not only environmentally benign, but also meets the requirements for sustainability. To the best of our knowledge, numerous and different strategies have emerged in recent years. For example, the addition of formic acid significantly promotes the yield of aromatics during the depolymerization of oxidized lignin, giving rise to a value of the yield over 60 *wt. %*.⁷ Moreover, treatment of lignin with formaldehyde protects side-chain hydroxyl groups, allowing for near-theoretical yields of aromatic products by hydrogenolysis.⁸ Recently, the selective production of diethyl maleate (DEM) was achieved by using polyoxometalate ionic liquid catalysts (POM ILs) to promote the selective oxidation of lignin coupled with esterification of the resulting aromatic monomers.⁹ Nevertheless, these processes still exhibit some drawbacks, for instance, high temperature, high H₂ pressure and long reaction time plague the heterogeneously catalyzed processes to realize both high lignin conversion and product yields, largely due to the poor contact between the macromolecule and catalyst. On the other hand, product separation and isolation can prove quite energy consuming and costly for systems employing homogeneous catalysts.¹⁰ Generally, process intensification and coupling techniques are a potential alternative to solve these problems,^{11,12} among which the emulsion approach has received a resurgence in interest recently. Because the emulsion system is able to provide a much larger interface for reactions involving in problem related with the incompatibility of reactants.¹³

As described above, lignin can be employed as a surfactant,^{4,14,15} or as a precursor for the production of functional surfactants due to the numerous hydrophilic and hydrophobic groups it contains.¹⁶ Hence, developing an emulsion system utilizing lignin as the surfactant has obvious advantages, and several new emulsion systems for lignin depolymerization have been demonstrated on the basis of its self-surfactivity. For example, over three times of phenolic monomers' yield has been obtained in a water/oil (W/O) emulsion reactor comparing to those in a standard solvent system.¹⁷ Basing on this work, a purpose-designed emulsion was utilized for the depolymerization of lignosulfonate to result in the generation of appreciable yields of phenolic monomers and 4-ethyl guaiacol, 116.1 and 39.3 mg g⁻¹ respectively.¹⁸ Furthermore, Wessling *et al.* proposed an emulsion system comprised of a deep eutectic solvent and an extractant for electrochemical oxidation of kraft lignin to low molecular weight products (ranging from 100 to 600 Da).¹⁹ The above examples make it clear that emulsion approaches can promote lignin depolymerization to some degree, yet higher lignin conversion facilitates a destabilization of the system and thus reduces process efficiency, although the demulsification can be seen as a kind of benefit due to the partitioning effect achieved after reaction.

To overcome the above difficulties, a surfactant-free microemulsion (SFME) system could be a better choice for the intensification of lignin depolymerization, due to its thermodynamic stability and much more larger interfacial area.²⁰ The SFME is more commonly referred to as a pre-Ouzo or detergentless microemulsion, so-called due to the spontaneous formation of a stable emulsion with only the addition of water, a property that is shared by Ouzo, a famous alcoholic beverage in Greece.^{21,22} Thus, SFMEs are known to have properties similar to those of surfactant-based microemulsions (SBMEs), providing both the solubilization effect and capacity to dissolve the immiscibility solvents,²³ but not need to separate the surfactant from the system,

showing great advantage both in cost and process.^{24,25} Herein, a novel oil/water (O/W) SFME containing octane, *n*-propanol and water was proposed after carefully screening, and the oxidative depolymerization of lignin in this SFME was conducted basing on the construction of the ternary diagram and the determination of lignin solubility distribution in its different subregions. Experimental results showed that around 40 to 500wt. % increase of phenolic monomers in SFME reactor was achieved with comparison to those in non-microemulsion systems, illustrating great potential to develop novel SFME for the valorization of biomass.

Materials

Dimethyl-1,2-benzenedicarboxylate, octane, *n*-propanol, and *p*-hydroxybenzaldehyde were provided from Aladdin, China. Ethyl acetate, ethanol, anhydrous sodium sulfate, copper sulfate, ferrous sulfate, zinc sulfate and magnesium sulfate were purchased from Tianjin Damao Chemical Reagent Factory, China. Sodium lignosulfonate and alkali lignin were supplied by Sigma-Aldrich, China. Organosolv lignin was obtained according to our previous study.²⁶ Briefly, 10.0 g biomass feedstock (bagasse, poplar, bamboo or miscanthus powers), 1.2 g concentrated H₂SO₄ (Guangzhou Chemical Reagent Factory, China) and 150 mL 80% ethanol solution were placed into a 250 mL stainless autoclave and heated to 393 K at a stirring speed of 600 rpm. After 4 h, the autoclave was cooled rapidly under flowing water. Then, the reaction mixture was filtered, the filtrate was added into 500 mL deionized water for precipitating lignin. The solid (organosolv lignin) obtained by filtration was then dried under vacuum at 313 K for 12 h before use.

Phase diagram construction

Phase diagram of octane/*n*-propanol/water ternary system was constructed at room temperature by titration and the detailed steps were as follows. At first, a mixture with the desired mass ratio of octane to water ($R_{O/W}$) was prepared in a dry beaker. Then, *n*-propanol was slowly dropped to it until the ternary mixture changed from turbidity to transparency under magnetic stirring. Repetition of the above steps for different $R_{O/W}$ values allowed the construction of the phase diagram, in which the component content is the average value obtained by repeating all processes at least three times.

Oxidation of Lignin

The oxidation of lignin was performed in a 50 mL autoclave (Labe Scientific Instrument Co., Ltd., Shanghai, China) with Teflon inner. In a typical reaction, 0.1 g lignin, desired amount of catalyst and 10 g pre-prepared microemulsion mixture were added in the autoclave, then 1.0 MPa O₂ was used to purge it three times and pressurized. Subsequently, the autoclave was heated and kept at a designated temperature for 1-5 h under the stirring rate of 600 rpm. After the reaction, the autoclave was cooled with flowing water to room temperature. The reaction mixture was diluted by ethanol to a fixed volume of 25 mL, among which 5 mL was fetched and dried by anhydrous sodium sulfate for GC-MS analysis. Then, 50 mL deionized water was added into other 20 mL solution for reprecipitating lignin. So recovered lignin (Re-lignin) was obtained by the filtration and then washed by water and dried for 4 h at 333 K for subsequent characterization.

Measurement and Characterization

The subregions of microemulsions were distinguished through electrical conductivity measurements (DDSJ-308A, DSJ-0.1C electrode, Shanghai Precision Scientific Instrument Co., Ltd). During analysis, suitable amount of acetic acid was added into the oil phase, with the concentration about 50 mmol L⁻¹.²⁷ The micro-polarities of different microemulsions using methyl orange (MO) as the probe and the solubility of lignin were measured by UV-vis spectroscopy (UV-2450, Shimadzu, Japan) at room temperature with 0.1 nm resolution. Lignin concentrations in different microemulsions were calculated by an external standard method, where every test was carried out in triplicate. Cryogenic scanning electron microscopy (Cryo-SEM) was performed on a JSM-7100F SEM (JEOL Ltd, Tokyo, Japan) at 133 K. Before analysis, the samples were pre-cooled by liquid nitrogen and stayed in the preparation chamber (PP3010T Cryo-SEM Preparation System, Quorum Technologies, UK) at 133 K. The formation of different microemulsions, and the structures of raw lignins and Re-lignin were characterized by FT-IR spectrophotometer (Bruker Tensor 27) by the KBr pellets with 4 cm⁻¹ resolution and 64 scan times.

Volatile products were identified by GC-MS (Agilent 7890B/5977A, HP-INNOWAX capillary column: 30 m \times 0.32 mm \times 0.25 μ m) on the base of Agilent MS library. The temperatures of the injection and detector were fixed to 553 K. The oven temperature was started at 323 K (held for 1 min), then programmed to 533 K at the rate of 10 K min⁻¹ and finally kept at 533 K for 15 min. The quantitative analysis was performed by GC (Agilent 7890B) equipped with a FID detector using the same chromatography column and temperature program as above GC-MS analysis. The yields of phenolic monomers were measured by using dimethyl phthalate as the internal standard and calculated through following equations:

$$Y = \frac{A_i M W}{A M_L} \times 1000 \text{ mg g}^{-1} \text{ (Equation 1)}$$

$$Y = \text{mg g}^{-1} \text{ (Equation 2)}$$

where Y_i and A_i are the yield and peak area of the product i , Y is the total yield of phenolic monomers. M and M_L represent the mass of internal standard solution and lignin (g), W and A represent the mass concentration and peak area of internal standard, respectively.

Result and Discussion

Phase behavior of the ternary system

Figure 1 shows the ternary diagram of octane/ n -propanol/water at room temperature, in which the component content is expressed as the mass fraction. It is clearly seen that there are two regions in the ternary diagram, *i.e.*, multiphase region and single-phase (microemulsion region). For the multiphase region, the ternary system is turbid liquid under stirring, and it transforms to two phases quickly after standing by for a few minutes. But, further addition of n -propanol makes this multiphase region shifting to single-phase, and the ternary system becomes optically isotropic and transparent, which are typical properties of microemulsion. So constructed diagram demonstrates clearly that the immiscible two phases of octane and water can become a stably homogeneous system in the presence of n -propanol with a suitable amount, by contrast, this similar phenomenon was shown in the previous study as well.²⁸ Interestingly, the continuous area of the single-phase region in this ternary system accounts for about 22% of the total phase diagram and the single-phase channel extends from oil-rich to water-rich region, hence, it is thought that this novel SFME system is suitable to examine the influence of the microemulsion structure transition on the depolymerization process.²⁰

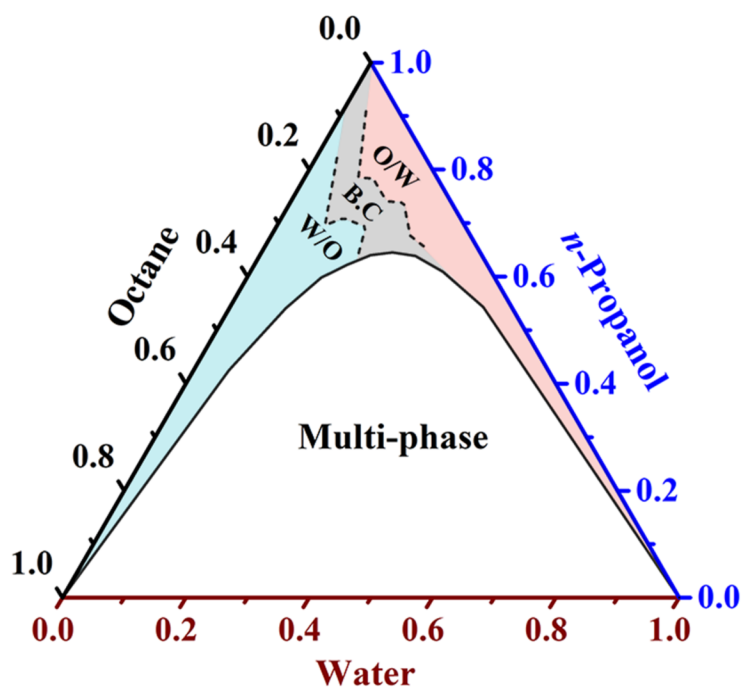


Figure 1. Ternary diagram of octane/*n*-propanol/water at room temperature.

Characterization of the microemulsion

The electrical conductivity (κ) of the microemulsion is sensitive to the change of its microstructure.^{29,30} Therefore, it is usually used to distinguish the subregions in the microemulsion. The variations of electrical conductivity with respect to the mass fraction of oil phase (W_{OA} , octane phase containing 50 mmol L⁻¹ acetic acid) at different mass ratios of *n*-propanol to water ($R_{P/W}$) are presented in Figure S1 and some typical results are shown in Figure 2A. It can be found that the κ value increases initially and then decreases with the increasing of W_{OA} value. For the purpose of clarity, the curve of κ with the increase of W_{OA} at fixed $R_{P/W}$ of 9.02 is taken as an example alone (Figure 2B). Obviously, there are two breaks at the tested W_{OA} values of 10.4 and 20.8 wt.%, which divide the curve into three stages. At the first stage, the initial increase of κ before the W_{OA} value reaching to 10.4 wt.% is attributed to the successive increase of the conductivity of oil/water (O/W) microemulsion droplets. This behavior can be further assigned to the continuous adding of octane into aqueous phase since the droplets can absorb the ions from water and the charges are generated by friction in the aqueous phase. Thus, the larger conductivity value with the increased W_{OA} indicates the formation of O/W microemulsion. Then, the electrical conductivity begins to decrease with further increase of W_{OA} , showing the generation of bicontinuous (B.C) microemulsion, where the O/W microemulsion droplets are broken by collision, and the oil phase also begins to aggregate to form network-like structures, which can be observed distinctly by the following Cryo-SEM image (Figure 5B). In this stage, an inverse relationship between electrical conductivity and octane concentration is observed. It is because the conductivity of this system depends on the conductive channels generated by the continuous water phase, where these channels became much narrower with the decline of water content. When the W_{OA} value exceeds 20.8 wt.%, the κ value decreases linearly with the increase of W_{OA} , which corresponds to the formation of water/oil (W/O) microemulsion. In this W/O microemulsion region, the continuous phase is octane and the κ value only relies on the movability of water micro-droplets, where the gradual disappearance of water droplets results in a linear decrease of κ value in this system with increasing W_{OA} (more than 20.8wt.%). Thus, the three subregions marked O/W, B.C and W/O of the single-phase region

shown in Figure 1 are distinguished clearly through electrical conductivity measurements.

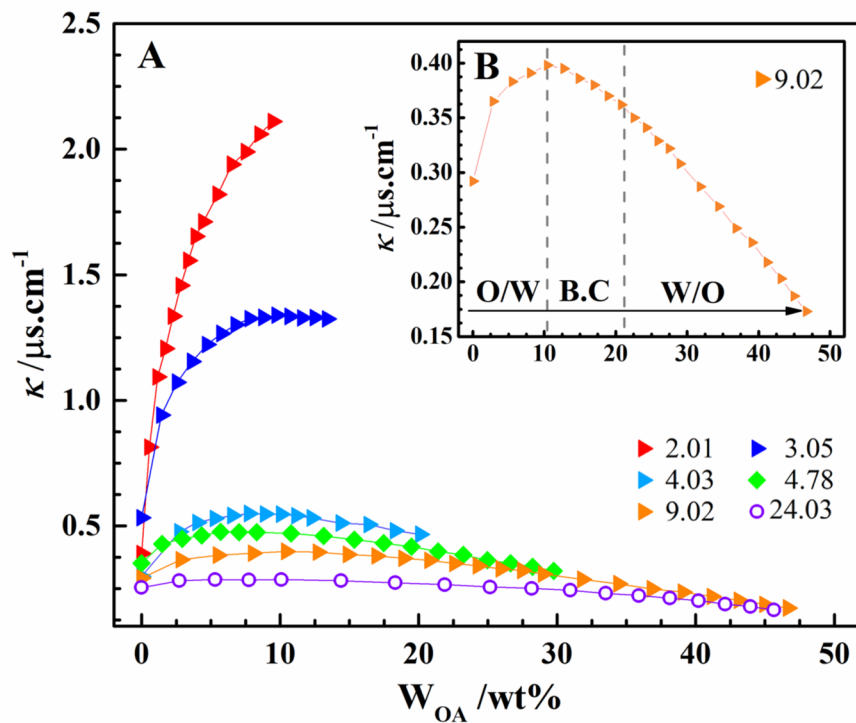


Figure 1: This is a caption

Figure 2. Conductivity κ as a function of octane content (W_{OA}) at (A) different $R_{P/W}$ values and (B) the fixed $R_{P/W}$ of 9.02 in the microemulsion.

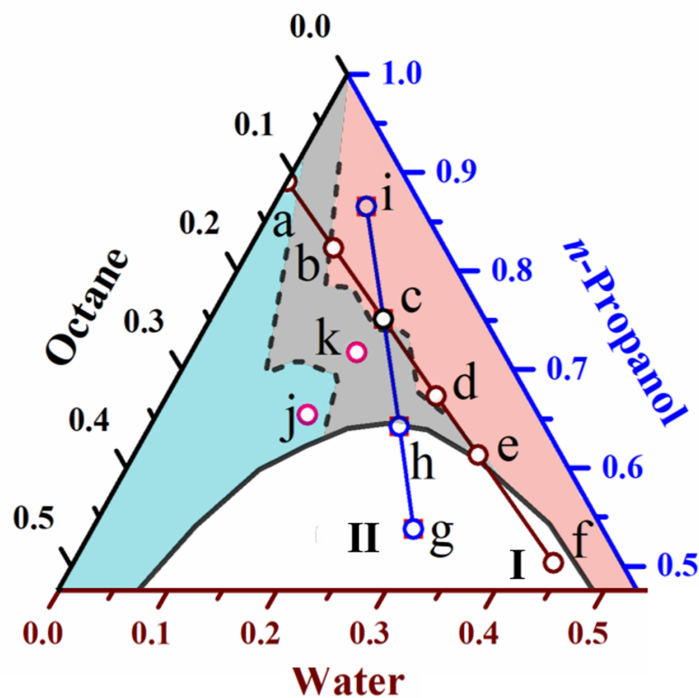
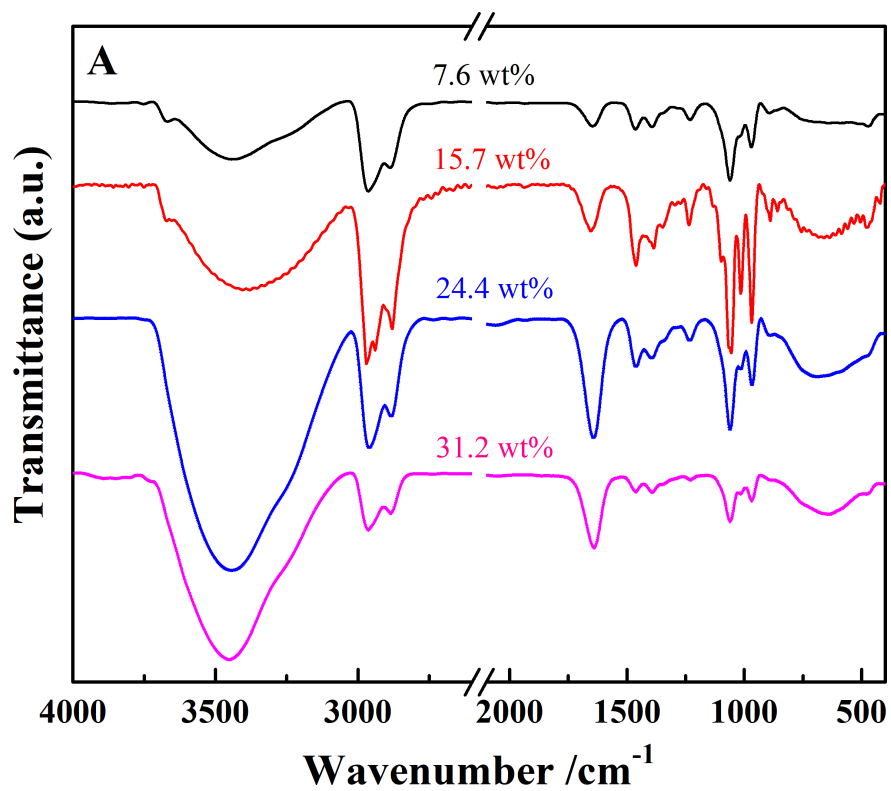


Figure 3. Different points located in the SFME system for characterization.

Furthermore, in this study, methyl orange (MO) is used as a probe for polarity measurements of the SFME system, as it is sensitive to that of the local micro-environment, giving a red shift on its maximum absorption wavelength (λ_{\max}) in a medium possessing higher polarity and vice versa.^{31,32} Therefore, the measurement of different microemulsions at the fixed $R_{P/O}$ value of 8.16 (Line I in Figure 3) was examined by UV-vis spectroscopy (Figure S2A). The results show that the λ_{\max} of MO exhibits a red-shift (from 416.3 to 421.9 nm) with an increase of water content (W_W), confirming the enhanced polarity of the microemulsion. At the same time, this linear increase in the λ_{\max} of MO with the increase of W_W indicates clearly that there is no change of microemulsion type in the test area and all the given systems are assigned to O/W microemulsions, this also validates the nature of the subregions determined above. Moreover, the polarity of the microemulsion at point c in Figure 3 is compared with those of common solvents (Figure S2B). It can be found that the λ_{\max} in pure water and *n*-propanol are centered at 464.8 and 414.6 nm, respectively, while it peaks at 422.0 nm in the binary system without octane at a $R_{P/W}$ value of 4.78. However, when a microemulsion with a $R_{P/W}$ value of 4.78 contains 9.2 wt. % octane (point c in Figure 3), the λ_{\max} of MO shifts to 419.2 nm. Therefore, the micro-polarity of the as-constructed microemulsion system exists between those of bulk water and *n*-propanol.

Moreover, the formation mechanism of different microemulsions was investigated using FT-IR analysis to obtain information about their intermolecular and intramolecular interactions.³³ The spectra of microemulsions with increasing W_W (Line I in Figure 3) are shown in Figure 4. There is only one strong and broad adsorption peak in the range of 3000 to 3800 cm^{-1} for each microemulsion system, which is attributed to the stretching vibration of hydroxyl groups. Interestingly, this adsorption peak is broadened and shifts to lower wave numbers with the increasing W_W (Figure 4A) and it can be contributed to the formation of hydrogen bonds by the addition of water.³⁴ In order to clearly demonstrate this effect, the hydroxyl band was deconvoluted using an appropriate method described by Gao *et al.*³⁵ Three distinct water species can be identified, *i.e.*, trapped-, bound- and free-water. According to the fitted results (Figure 4B), trapped-water (*ca.* 3610 cm^{-1}) exists as a comparatively small fraction in this system and is considered to be dissolved in octane or

bonded with the alkyl chain of the *n*-propanol molecule. The bound-water (*ca.* 3480 cm^{-1}) is identified as forming hydrogen bonds with the hydroxyl group of *n*-propanol. The absorbance observed at 3348 cm^{-1} is characterized as belonging to the O-H stretching vibration of *n*-propanol, and the one centered at 3210 cm^{-1} is assigned to that of free water due to the formation of strong hydrogen bonds among themselves.³⁶



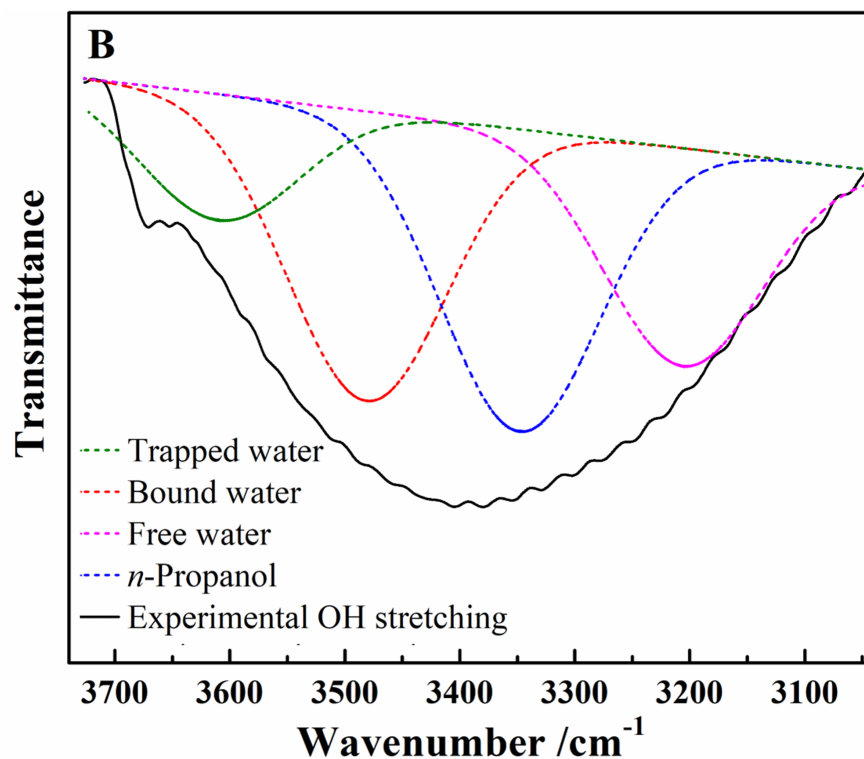


Figure 4. FT-IR spectra diagram of (A) different solvents with $R_{P/O}=8.16$ and (B) the fitted curve and the experimental one of the OH stretching band at $W_W=15.7 \text{ wt.}\%$.

Solubility of lignin in microemulsion system

However, the solubilization effect is one of the most important features of the microemulsion system, therefore the solubilities of lignin in different microemulsions were measured and listed in Table 1. The lignin sample originated from bagasse is insoluble in both water and octane (Table 1, entries 1 and 2), but it can dissolve in *n*-propanol with the solubility of 19.9 g L^{-1} (Table 1, entry 3). Basing on the above constructed SFME system and the recognition of its subregion, the solubilities of lignin in different microemulsions were investigated. At first, different O/W microemulsions at a fixed $R_{P/O}$ value of 8.16 were selected to test the effect of water content (Table 1, entries 4-8), considering that water is a kind of green and easily available solvent. The solubility of lignin in the *n*-propanol/octane system without water (Table 1, entry 4, point a in Figure 3) is close to that in *n*-propanol. However, due to the solubilization effect and the changing polarity of microemulsions, the solubility of lignin is enhanced significantly by adding water to the *n*-propanol/octane system. For example, when the W_W value increases from 7.6 to 15.7 wt. %, the solubility of lignin sharply rises from 28.6 to 79.1 g L^{-1} (Table 1, entries 5 and 6, points b and c in Figure 3), which is compatible to that obtained in ionic liquids.^{37,38} And it remains about 71.9 g L^{-1} when the W_W value further increases to 31.2 wt. % (Table 1, entries 7 and 8, points d and e in Figure 3). It implies that suitable polarity for the microemulsion may act as an important parameter to affect the solubility of lignin, because the polarity of the microemulsion increases with the elevated W_W value as illustrated in Figure S2A, while lots of polar groups in lignin macromolecules also provide contribution to the solubilization. In order to give a more understanding about the solubilization effect in all subregions, the solubility of lignin affected by *n*-propanol content (W_P) was further determined under the fixed mass ratio of water to octane ($R_{W/O}$) basing on the maximum value obtained above (Table 1, entries 6, 9 and 10, points c, f and g in Figure 3). The solubility of lignin sharply increases at first and then decreases slightly with the increase of W_P , and it reaches the maximum value at the W_P value of 75.1 wt. %, which is the same point as mentioned above.

Besides, it is worth noticing that the solubilities of lignin in the most given O/W microemulsions improve greatly, compared with those in B.C and W/O microemulsions (Table 1, entries 9 and 11, points f and j in Figure 3). More interestingly, all the solubilities of lignin in the given microemulsions are larger than that in *n*-propanol or *n*-propanol/octane binary system under the same conditions (Table 1, entries 5-11 vs 3 and 4), this does verify enhanced solubilization of the microemulsions. Therefore, the microemulsion possesses the best solubility for lignin is regarded largely with the composition of 15.7 wt. % water, 9.2wt. % octane and 75.1 wt. % *n*-propanol, exhibiting about four times of the lignin solubility in comparison to that in *n*-propanol.

Table 1 . Solubility of lignin in different microemulsions

Entry	Solvent /wt.%	Solvent /wt.%	Solvent /wt.%	Microemulsion type	Solubility /g L ⁻¹
	Water	Octane	<i>n</i> -Propanol		
1	100	-	-	-	-
2	-	100	-	-	-
3	-	-	100	-	19.9
4	-	10.9	89.1	-	20.1
5	7.6	10.1	82.3	O/W	28.6
6	15.7	9.2	75.1	O/W	79.1
7	24.4	8.2	67.4	O/W	73.6
8	31.2	7.5	61.3	O/W	71.9
9	22.6	13.2	64.2	B.C	57.0
10	8.5	5.0	86.5	O/W	45.8
11	13.7	20.9	65.4	W/O	42.1

Condition: at room temperature.

In order to give an intuitionistic understanding about the droplets and micro-structures of microemulsions in the SFME system, cryogenic scanning electron microscopy (Cryo-SEM) was performed according to previous reports,^{39, 40} and conducted on the above microemulsion systems (points c, k and j in Figure 3) dissolving with or without lignin from different subregions. It is clear to see the existence of the discrete spherical droplets in the O/W microemulsion system containing lignin (point c in Figure 3), where the average diameter of the droplets is about 67 nm (Figure 5A and Figure S3A). Figure 5B shows the micro-structure of B.C microemulsion (point k in Figure 3) in presence of lignin. The obvious sponge-like structures, which are generated owing to the break of microemulsion droplets alongside the interconnections between two phases, are considered to be the feature structure of B.C microemulsion. The Cryo-SEM image of W/O microemulsion (point j in Figure 3) with lignin is also exhibited (Figure 5C) and the average diameter of its droplets is around 50 nm (Figure S3B). These Cryo-SEM images verify visually that the O/W, B.C and W/O microemulsions are formed orderly with the increase of octane content (W_O) when the $R_{P/W}$ is fixed at 4.78. Furthermore, the above O/W microemulsion without lignin was also compared (Figure 5D). Surprisingly, the size of its droplets becomes to the smallest one with an average diameter of 48 nm (Figure S3C).

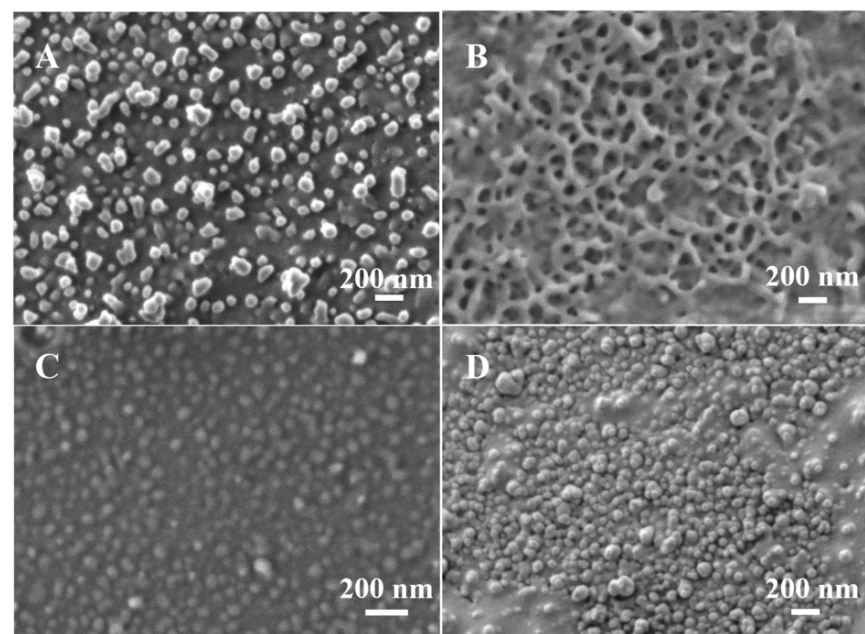


Figure 5. Cryo-SEM images as a function of W_O in the microemulsion with lignin at fixed $R_{P/W}$ value of 4.78 with different W_O value (*wt. %*) of (A) 9.2, (B) 13.3, (C) 20.9, and (D) without lignin in (A).

Hence, it suggests that lignin macromolecules are able to facilitate the formation of bigger and discrete microemulsion droplets, and then to have this SFME system stabilized due to the aggregation of amphipathic lignin at the surface of the microemulsion droplets, which can improve the contact between lignin and hydrosoluble catalyst for the following lignin oxidation. Additionally, by comparison the microemulsion droplets with and without lignin, the size distribution of the former is less concentrated than that of the later (Figure S3C), which can be attributed to the high dispersion degree of lignin macromolecule (Table S1), resulting a wider size distribution of droplets in the microemulsion with lignin.

Oxidation of lignin in microemulsion reactor

Basing on the constructed microemulsion system and the above characterizations, the lignin oxidation performance in the microemulsion system using water soluble CuSO_4 as the catalyst was investigated (Table 2). In this study, the products from lignin oxidation are classified to *p*-hydroxyphenyl (H), guaiacyl (G) and syringyl (S) alcohol unit products according to their structure as it is widely accepted that lignin mainly contains these structural units.⁵ The oxidation of lignin in common solvents was conducted firstly for the comparison. The results show that the total yields of phenolic monomers are far from desired value when water, octane and *n*-propanol are used as the solvent correspondingly (Table 2, entries 1-3), where only 22.5 mg g^{-1} of phenolic monomers is produced in *n*-propanol, which can be ascribed to the limited solubility of lignin in *n*-propanol (Table 1, entry 3). Besides, the improved yields of phenolic monomers in the binary systems imply that the addition of octane or water to *n*-propanol can promote the oxidation of lignin (Table 2, entries 4 and 5). However, there is no obvious increase of phenolic monomers in the given ternary systems located in multiphase region (Table 2, entries 6 and 7), the limited solubility of lignin in these multiphase emulsions can be responsible for this situation. But interestingly, the yield of phenolic monomers in the microemulsion reaches to 90.2 mg g^{-1} (Table 2, entry 8, point c in Figure 3), which gives about 40 to 500 *wt. %* increment to those of above solvents, indicating that the formation of microemulsion can significantly intensify this lignin oxidation process. Additionally, the oxidation of lignin in the above microemulsion in the absence of catalyst was also studied (Table 2, entry 9). It gives 46.2 mg g^{-1} of phenolic monomers, but no products from H, G and S units are detected, which conforms both the thermal and the above solubilization effects during lignin depolymerization.

As mentioned, the highest yield of phenolic monomers is obtained from the above microemulsion (Table 2, entry 8, point c in Figure 3). Therefore, the mass ratio of *n*-propanol to octane in microemulsion was fixed for investigating the influence of W_W (points a-f in Figure 3) during lignin depolymerization (Table 2, entries 8 and 10-13). It can be found that the yield of phenolic monomers increases significantly at first and then has a slight fluctuation with the increase of W_W in the microemulsion region. For example, it is 32.6 mg g^{-1} in the absence of water, while it reaches to the maximum of 90.2 mg g^{-1} at the W_W of 15.7 wt. \% (Table 2, entry 8, point c in Figure 3). Incidentally, the yields of products from the transformation of H, G and S units reach to their peak values at the W_W of 15.7 , 24.4 and 31.2 wt. \% , respectively (Table 2, entries 8, 12 and 13, points c-e in Figure 3). Whereas, there is an obvious decrease in phenolic monomer products when the W_W further increases to 43.8 wt. \% (Table 2, entry 14, point f in Figure 3). This decline can be attributed to the great decrease of interfacial area and the increase of mass transfer resistance in this multiphase emulsion compared with those in microemulsions. Similarly, the influence of W_P in the microemulsion with the fixed $R_{W/O}$ of 1.71 (Line II in Figure 3) on the lignin oxidation process was also investigated (Table 2, entries 8 and 15-17). The yield of phenolic monomers is only 59.7 mg g^{-1} at the W_P value of 53.8 wt. \% (Table 2, entry 15, point g in Figure 3), which is partially because this ternary system locates in the multiphase region. Interestingly, the yield of phenolic monomers reaches to the peak value when the W_P value increases to 75.1 wt. \% , the same point as mentioned above. But it drops to 67.8 mg g^{-1} when the W_P value further increases to 86.5 wt. \% (Table 2, entry 18, point i in Figure 3). This can also be ascribed to the change of phase behavior and lignin solubility in the investigated system (Table 1, entry 6). It should be noticed that the constructed B.C and W/O microemulsions have similar efficiency (Table 2, entries 16 and 18, points h and j in Figure 3) for lignin oxidation compared with those of traditional solvent systems, while most of the given O/W microemulsions can promote the oxidation of lignin rationally. In belief, the type and component ratio of microemulsion are considered as the key factors for this oxidation process. But, it is interesting to point that the yields of products from the H unit are at least twice or triple to those from the G or S unit, although the ratio of H unit in lignin is the lowest, while the content of H, G and S units in bagasse lignin are 15, 45 and 40% respectively,⁴¹ demonstrating that these systems are prefer to oxidize H unit rather than other units.

Table 2. Effect of different solvents on the oxidation of lignin.

Entry	System /wt.%	System /wt.%	System /wt.%	System /wt.%	Yield /mg g ⁻¹	Yield /mg g ⁻¹	Yield /mg g ⁻¹
	Water	Octane	<i>n</i> -Propanol	Microemulsion type	H	G	S
1	100	0	0	-	10.5	3.6	-
2	0	100	0	-	-	-	-
3	0	0	100	-	16.1	6.4	-
4	0	50.0	50.0	-	23.5	7.8	1.2
5	50.0	0	50.0	-	42.7	12.5	2.2
6	33.3	33.4	33.3	-	45.9	6.9	2.2
7	25.0	25.0	50.0	-	40.5	15.7	4.9
8	15.7	9.2	75.1	O/W	60.9	23.7	5.6
9 ^a	15.7	9.2	75.1	O/W	-	-	-
10	0	10.9	89.1	-	12.4	10.1	-
11	7.6	10.1	82.3	O/W	36.0	18.0	5.3
12	24.4	8.2	67.4	O/W	50.4	25.1	6.2
13	31.2	7.5	61.3	O/W	51.2	21.8	10.9
14	43.8	6.1	50.1	-	38.0	12.2	0.6
15	29.2	17.0	53.8	-	41.1	16.0	2.6
16	22.6	13.2	64.2	B.C	35.2	17.7	2.9
17	8.5	5.0	86.5	O/W	33.3	16.7	4.0
18	13.7	20.9	65.4	W/O	34.7	15.8	3.1

Reaction condition: 10 g solvent, 1.0 wt. % lignin, 0.1 mmol CuSO₄, 1.0 MPa O₂, 433 K, 4 h. Note: H, G and S represent the products from the structural units of the *p*-coumaryl alcohol (H), coniferyl alcohol (G), and sinapyl alcohol (S) in lignin respectively. a-without CuSO₄.

Additionally, the structures of raw lignin and Re-lignins from different oxidation system were analyzed by FT-IR spectra (Figure 6). The absorbances at 3450 and 2912 cm⁻¹ can be assigned to the vibration of O-H and C-H stretching respectively, and those at 1605, 1514, 1454 and 814 cm⁻¹ are ascribed to the aromatic skeletal vibrations of lignin,⁴² which suggests that the skeletal structure of lignin is retained in Re-lignins. It is worth pointing out that the absorbance at 1740 and 1103 cm⁻¹ (characteristic absorption of C=O stretching and the H structural unit in lignin respectively) for Re-lignins from the microemulsion (point c in Figure 3) are weakened more significantly by comparison to that from other system, this observation further certifies that the developed microemulsion reactor is selective to tailor H unit in lignin.

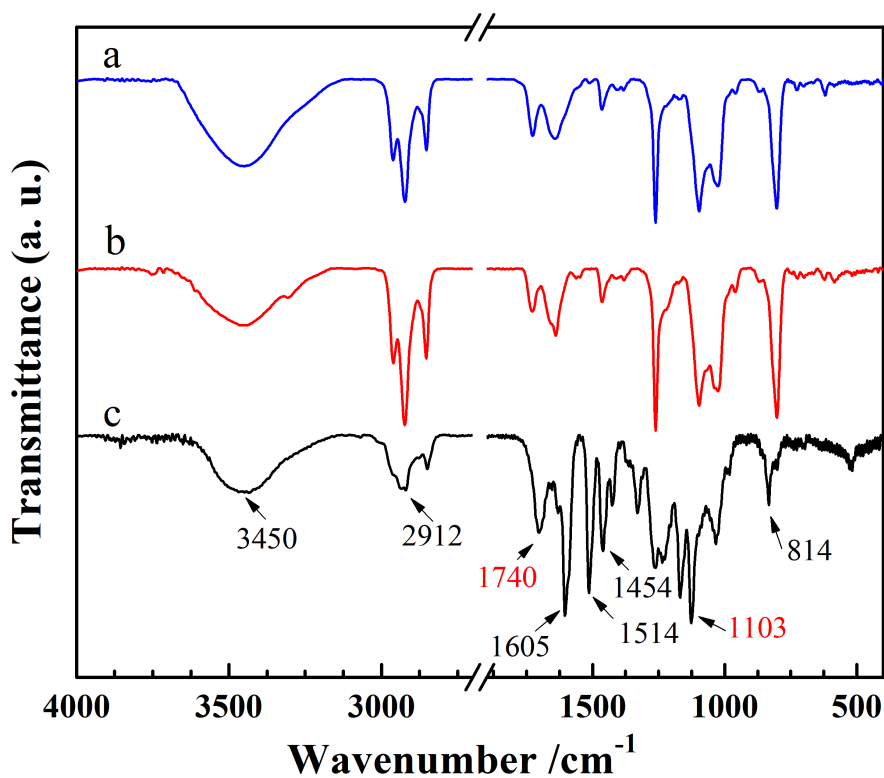


Figure 6. FT-IR spectra of recovered lignin from reaction system composed by water, octane and *n*-propanol with mass rate of (a) 25.0 :25.0 :50.0; (b) 15.7 :9.2 :75.1; and (c) raw lignin.

Comparison of different metal sulfate catalysts

In this study, the role of a series of metal sulfate catalysts on the oxidative lignin depolymerization was evaluated preliminarily. The effect of H₂SO₄ on the oxidation of lignin was considered in the present of CuSO₄ (point c in Figure 3), as it has reported that Brønsted acid is an effective promoter for lignin oxidation.⁴³ Experimental results exhibit that the existence of H₂SO₄ (12.5 mmol L⁻¹) in the microemulsion system does promote the oxidation of lignin and enhance the yield of phenol monomers (61.9 to 89.3 mg g⁻¹, Table 3, entries 1 and 4). Therefore, the above microemulsion containing 12.5 mmol L⁻¹ H₂SO₄ was used while other cheaper and water-soluble metal sulfates with divalent cations (CuSO₄, MgSO₄, ZnSO₄ and FeSO₄) were used with consideration to the salt effect of the microemulsion (Table 3, entries 2-6). The yield of phenolic monomers is 69.2 mg g⁻¹ in the presence of FeSO₄, but much higher yields are provided by CuSO₄ and ZnSO₄ (89.3 and 88.9 mg g⁻¹ respectively), while the highest yield of *p*-hydroxy benzaldehyde

(32.2 mg g⁻¹) is achieved in the presence of CuSO₄ (Table 3, entries 4 and 5). These differences between metal sulfates can be attributed to the different redox potential of metal cations.⁴⁴ However, there is negative effect for lignin oxidation in the acidic condition under the catalysis of MgSO₄, because it belongs to alkali salt (Table 3, entry 6). Besides, the influence of metal sulfates with monovalent and trivalent cations (Na₂SO₄ and Fe₂(SO₄)₃) to lignin oxidation was also investigated (Table 3, entries 7 and 8). But they both show much lower catalytic activity than that of CuSO₄. It should be noticed that the yield of phenolic monomers in the present of Fe₂(SO₄)₃ is lower than that of FeSO₄, which will be oxidized completely to Fe₂(SO₄)₃ at the atmosphere of O₂ (Table 3, entries 3 and 8). This difference can be considered to trigger more serious peroxidation of products under the catalysis of Fe₂(SO₄)₃.

Table 3. Comparison of metal sulfates on lignin oxidation in the microemulsion.

Entry	Catalyst	C _{H2SO4} /mmol L ⁻¹	Yield /mg g ⁻¹		
			HB	PHB	Total
1	-	12.5	27.9	-	62.1
2	CuSO ₄	-	18.2	6.6	61.9
3	FeSO ₄	12.5	21.8	23.6	69.2
4	CuSO ₄	12.5	32.2	13.0	89.3
5	ZnSO ₄	12.5	18.2	8.8	88.4
6	MgSO ₄	12.5	14.3	-	50.0
7	Na ₂ SO ₄	12.5	5.0	10.8	62.5
8	Fe ₂ (SO ₄) ₃	12.5	15.9	22.0	45.2

Reaction condition: 1.0 wt. % lignin, 10 g microemulsion (W_W :W_O :W_P = 15.7 :9.2 :75.1, wt. %), 0.1 mmol catalyst, 1 MPa O₂, 413 K, 4 h. Note: HB-*p* - hydroxybenzaldehyde; PHB- propyl-4-hydroxybenzoate.

Effect of process parameters and the capacity of the microemulsion reactor

In order to achieve the maximum yield of phenolic monomers and representative products, the process parameters such as reaction temperature, time and the amount of catalyst were optimized by using the microemulsion system located at point c (Figure 3). Results (Figure S4) show that the reaction temperature and time have similar effect and tendency on the oxidation of lignin, the maximum yield is obtained at 433 K for 4 h, achieving 119.9 mg g⁻¹ of phenolic monomers and generating two typical value added chemicals, *i.e.* ,*p*-hydroxy benzaldehyde and propyl-4-hydroxybenzoate with the yield of 48.2 and 21.2 mg g⁻¹ respectively. In addition, the dosages of CuSO₄ and H₂SO₄ for lignin oxidation in this system were also investigated (Figure S5) and the optimized dosages of CuSO₄ and H₂SO₄ are 0.1 mmol and 25.0 mmol L⁻¹ respectively. It is interesting to note that the changing trends of *p*-hydroxy benzaldehyde and propyl-4-hydroxybenzoate in Figure S5b are opposite, it suggests that the excess of H₂SO₄ can promote the oxidation of *p*-hydroxy benzaldehyde to *p*-hydroxybenzoic acid, which can be esterified easily with *n*-propanol under the acidic condition.

In addition, the oxidation performance of this microemulsion system for technical and organosolv lignins from different resources was studied under the optimized conditions and results are summarized in Table S2. It can be found that this microemulsion system is also appropriate to depolymerize other organosolv lignins into aromatic compounds. 101.2 and 109.1 mg g⁻¹ of phenolic monomers can be produced when bamboo and miscanthus organosolv lignins are used as the substrates respectively, while it provides 84.8 mg g⁻¹ yield over poplar organosolv lignin. It implies that herbaceous lignins are much easier to be depolymerized than hard wood lignins, due to less H unit containing in hard wood lignins,⁴⁵ which accords well with the above results about the selective tailoring of H unit. Besides, the yields of phenolic monomers from technical lignins are lower than those of organosolv lignins, in line with the more plentiful C-C bond containing structure of technical lignins.⁵ Quantitative analysis of volatile chemicals derived from bagasse organosolv lignin oxidation under the optimized conditions is exhibited in Figure S6 and Table S3. There are 12.7 wt. % of phenolic

products, including 52.4, 44.8 and 2.8% of H, G and S unit products. From this perspective, it can imply that H unit in lignin can be depolymerized easily, followed by the order of H > G > S unit in this case.

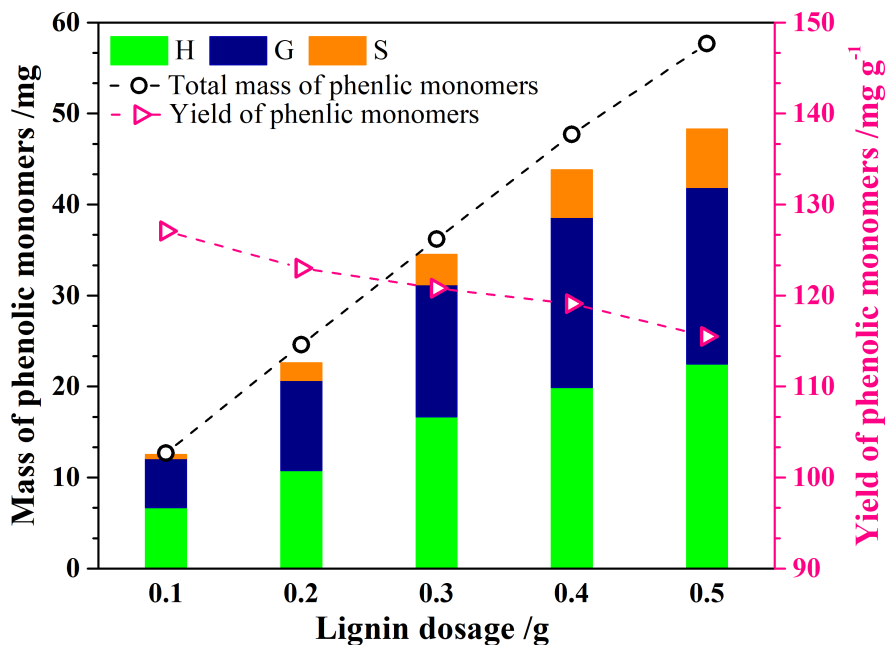


Figure 7. Effect of lignin dosage on the oxidation reaction.

Reaction condition: 10 g (12 mL) microemulsion ($W_W:W_O:W_P = 15.7:9.2:75.1, wt. \%$), 0.1 mmol $CuSO_4$, 25.0 mmol L^{-1} H_2SO_4 , 1 MPa O_2 , 433 K, 4 h.

The effect of initial lignin dosage on its own oxidation in the microemulsion reactor (point c in Figure 3) was studied to investigate the capacity of this novel reactor under the optimized reaction conditions. It is clearly seen in Figure 7, that the total mass of phenolic monomers grows linearly with the increasing mass of lignin. When the lignin dosage changes from 0.1 to 0.5 g, the total mass of phenolic monomers grows from 12.7 to 57.7 mg, while the loss of total yield of phenolic monomers is no more than 10% (127.1 to 115.1 $mg g^{-1}$). This demonstrates that this SFME reactor is efficient with a remarkable capacity up to 40.8 $g L^{-1}$ at 0.5 g lignin dosage, even by the comparison to the outstanding works about the oxidation of lignin in ionic liquid or aqueous system (12.5 and 10 $g L^{-1}$ respectively).^{9, 46} Moreover, by consideration of lignin solubility in this system (79.1 $g L^{-1}$), the capacity of the microemulsion reactor can be much higher for lignin oxidation, since the maximum concentration (40.8 $g L^{-1}$) is just near to half of its solubility in this study.

Conclusion

Microemulsion reactor was used for lignin depolymerization in this work for the first time, and the constructed octane/*n*-propanol/water SFEM system has a much better efficiency by comparison with typical solvent systems where 127.1 $mg g^{-1}$ of phenolic monomers is achieved under the optimized conditions. Characterizations by UV-vis spectroscopy, FT-IR spectroscopy and Cryo-SEM indicate that the solubility of lignin can be enhanced greatly in this microemulsion, and the microemulsion droplets are enlarged from 48 to 75 nm by the addition of lignin, due to the directional aggregation of lignin at the interface of microemulsion, thereby to have this lignin depolymerization process intensified. Furthermore, this system is appropriate for other organosolv lignins oxidation and the performance of it is stable even when lignin concentration is up to 40.8 $g L^{-1}$. Therefore, so constructed SFEM system can give a well example for highly efficient depolymerization of lignin through a novel reactor and simple process intensification strategy.

Acknowledgments

The authors gratefully acknowledge the financial support of the Natural Science Foundation of China (Grant No. 21736003, 21922813 and 21690083) and the Science and Technology Program of Guangzhou, China (201804020014).

References

1. Liu WJ, Li WW, Jiang H, Yu HQ. Fates of chemical elements in biomass during its pyrolysis. *Chem Rev* . 2017;117:6367-6398.
2. Zhang ZR, Song JL, Han BX. Catalytic transformation of lignocellulose into chemicals and fuel products in ionic liquids. *Chem Rev* . 2017;117(10):6834-6880.
3. Asgher M, Ahmad Z, Iqbal HMN. Alkali and enzymatic delignification of sugarcane bagasse to expose cellulose polymers for saccharification and bio-ethanol production. *Ind Crop Prod* . 2013;44:488-495.
4. Aro T, Fatehi P. Production and application of lignosulfonates and sulfonated lignin. *ChemSusChem* . 2017;10:1861-1877.
5. Zakzeski J, Bruijninx PCA, Jongerijs AL, Weckhuysen BM. The catalytic valorization of lignin for the production of renewable chemicals. *Chem Rev* . 2010;110:3552-3599.
6. Deepa AK, Dhepe PL. Lignin depolymerization into aromatic monomers over solid acid catalysts. *ACS Catal* . 2015;5:365-379.
7. Rahimi A, Ulbrich A, Coon JJ, Stahl SS. Formic acid-induced depolymerization of oxidized lignin to aromatics. *Nature* . 2014;515:249-252.
8. Shuai L, Amiri MT, Questell-Santiago YM, Héroguel F, Li YD, Kim H, Meilan R, Chapple C, Ralph J, Luterbacher JS. Formaldehyde stabilization facilitates lignin monomer production during biomass depolymerization. *Science* . 2016;354(6310):329-333.
9. Cai ZP, Long JX, Li YW, Ye L, Yin BL, France LJ, Dong JC, Zheng LR, He HY, Liu SJ, Tsang SCE, Li XH. Selective production of diethyl maleate via oxidative cleavage of lignin aromatic unit. *Chem* . 2019;5(9):2365-2377.
10. Behling R, Valange S, Chatel G. Heterogeneous catalytic oxidation for lignin valorization into valuable chemicals: what results? What limitations? What trends? *Green Chem* . 2016;18:1839-1854.
11. Olivier G, Pouya H, Faïcal L. Magnetically induced agitation in liquid-liquid-magnetic nanoparticle emulsions: potential for process intensification. *AIChE J* . 2014;60(3):1176-1181.
12. Stankiewicz A, Moulijn JA. Process intensification. *Ind Eng Chem Res* . 2002;41(8):1920-1924.
13. Timko MT, Smith KA, Danheiser RL, Steinfel JI, Tester JW. Reaction rates in ultrasonic emulsions of dense carbon dioxide and water. *AIChE J* . 2006;52(3):1127-1141.
14. Trufanova MV, Parfenova LN, Yarygina ON. Surfactant properties of lignosulfonates. *Russ J Appl Chem* . 2010;83(6):1096-1098.
15. Qiu XQ, Kong Q, Zhou MS, Yang DJ. Aggregation behavior of sodium lignosulfonate in water solution. *J Phys Chem B* . 2010;114:15857-15861.
16. Zhou HF, Lou HM, Yang DJ, Zhu JY, Qiu XQ. Lignosulfonate to enhance enzymatic saccharification of lignocelluloses: role of molecular weight and substrate lignin. *Ind Eng Chem Res* . 2013;52:8464-8470.
17. Cai ZP, Li YW, He HY, Zeng Q, Long JX, Wang LF, Li XH. Catalytic depolymerization of organo-solv lignin in a novel water/oil emulsion reactor: lignin as the self-surfactant. *Ind Eng Chem Res* . 2015;54:11501-11510.
18. Liu SJ, Lin ZY, Cai ZP, Long JX, Li ZM, Li XH. Selective depolymerization of lignosulfonate via hydrogen transfer enhanced in an emulsion microreactor. *Bioresource Technol* . 2018;264:382-386.
19. Marino DD, Aniko V, Stocco A, Kriescher S, Wessling M. Emulsion electro-oxidation of kraft lignin. *Green Chem* . 2017;19:4778-4784.
20. Xu J, Yin AL, Zhao JK, Li DX, Hou WG. Surfactant-free microemulsion composed of oleic acid, *n*-propanol and H₂O. *J Phys Chem B* . 2013;117:450-456.
21. Vitale SA, Katz JL. Liquid droplet dispersions formed by homogeneous liquid-liquid nucleation: “The Ouzo effect”. *Langmuir* . 2003;19:4105-4110.
22. Lund G, Holt SL. Detergentless water/oil microemulsions: IV. the ternary pseudo-phase diagram for and properties of the system toluene/2-propanol/water. *JAOCs* . 1980;57:264-267.

23. Klossek ML, Touraud D, Zemb T, Kunz W. Structure and solubility in surfactant-free microemulsions. *Chem Phys Chem* . 2012;13:4116-4125.
24. Hou WG, Xu J. Surfactant-free microemulsions. *Curr Opin Colloid In* . 2016;25:67-74.
25. Zoumpanioti M, Karali M, Xenakis A, Stamatias H. Lipase biocatalytic processes in surfactant free microemulsion-like ternary systems and related organogels. *Enzyme Microb Tech* . 2006;39:531-539.
26. Long JX, Li XH, Guo B, Wang LF, Zhang N. Catalytic delignification of sugarcane bagasse in the presence of acidic ionic liquids. *Catal Today* . 2013;200:99-105.
27. Zhang YM, Chen XL, Liu XF. Temperature-induced reversible-phase transition in a surfactant-free microemulsion. *Langmuir* . 2019;35:14358-14363.
28. Song F, Xu J, Hou WG. Surfactant-free oil/water and bicontinuous microemulsion composed of benzene, ethanol and water. *Chinese Chem Lett* . 2010;21:880-883.
29. Gao YN, Wang SQ, Zheng LQ, Han SB, Zhang X, Lu DM, Yu L, Ji YQ, Zhang GY. Microregion detection of ionic liquid microemulsions. *J Colloid Interf Sci* . 2006;301:612-616.
30. Song MM, Liu WJ, Wang Q, Wang J, Chai JL. A surfactant-free microemulsion containing diethyl malonate, ethanol, and water: microstructure, micropolarity and solubilizations. *J Ind Eng Chem* . 2020;83:81-89.
31. Sun B, Chai JL, Chai ZQ, Zhang XY, Cui XC, Lu JJ. A surfactant-free microemulsion consisting of water, ethanol, and dichloromethane and its template effect for silica synthesis. *J Colloid Interf Sci* . 2018;526:9-17.
32. Xu J, Deng HH, Fu YL, Chen YQ, Zhang J, Hou WG. Surfactant-free microemulsions of 1-butyl-3-methylimidazolium hexafluorophosphate, propylamine nitrate, and water. *Soft Matter* . 2017;13:2067-2074.
33. Clarke MJ, Harrison KL, Johnston KP, Howdle SM. Water in supercritical carbon dioxide microemulsions: spectroscopic investigation of a new environment for aqueous inorganic chemistry. *J Am Chem Soc* . 1997;119:6399-6406.
34. Luo T, Zhang JL, Tan XN, Liu CC, Wu TB, Li W, Sang XX, Han BX, Li ZH, Mo G, Xing XQ, Wu ZH. Water-in-supercritical CO₂ microemulsion stabilized by a metal complex. *Angew Chem Int Ed* . 2016;55:13533-13537.
35. Gao YA, Li N, Zheng LQ, Bai XT, Yu Li, Zhao XY, Zhang J, Zhao MW, Li Z. Role of solubilized water in the reverse ionic liquid microemulsion of 1-butyl-3-methylimidazolium tetrafluoroborate/TX-100/benzene. *J Phys Chem B* . 2007;111:2506-2513.
36. Zhou GW, Li GZ, Chen WJ. Fourier transform infrared investigation on water states and the conformations of aerosol-OT in reverse microemulsions. *Langmuir* . 2002;18:4566-4571.
37. Hart WES, Harper JB, Aldous L. The effect of changing the components of an ionic liquid upon the solubility of lignin. *Green Chem* . 2015;17:214-218.
38. Glas D, Doorslaer CV, Depuydt D, Liebner F, Rosenau T, Binnemans K, Vos DED. Lignin solubility in non-imidazolium ionic liquids. *J Chem Technol Biotechnol* . 2015;90:1821-1826.
39. Ben-Barak I, Talmon Y. Direct-imaging cryo-SEM of nanostructure evolution in didodecyldimethylammonium bromide-based microemulsions. *Z Phys Chem* . 2012;226:665-674.
40. Davidovich I, Issman L, Paula CD, Ben-Barak I, Talmon Y. A cryogenic-electron microscopy study of the one-phase corridor in the phase diagram of a nonionic surfactant-based microemulsion system. *Colloid Polym Sci* . 2015;293:3189-3197.
41. Ma HW, Li HW, Zhao WJ, Li LX, Liu SJ, Long JX, Li XH. Selective depolymerization of lignin catalyzed by nickel supported on zirconium phosphate. *Green Chem* . 2019;21:658-668.
42. Long JX, Lou WY, Wang LF, Yin BL, Li XH. [C₄H₈SO₃Hmim]HSO₄ as an efficient catalyst for direct liquefaction of bagasse lignin: decomposition properties of the inner structural units. *Chem Eng Sci* . 2015;122:24-33.
43. Imai T, Yokoyama T, Matsumoto Y. Revisiting the mechanism of β -O-4 bond cleavage during acidolysis of lignin IV: dependence of acidolysis reaction on the type of acid. *J Wood Sci* . 2011;57:219-225.
44. Werhan H, Mir JM, Voithl T, Rohr PRV. Acidic oxidation of kraft lignin into aromatic monomers catalyzed by transition metal salts. *Holzforschung* . 2011;65(5):703-709.

45. Partenheimer W. The aerobic oxidative cleavage of lignin to produce hydroxyaromatic benzaldehydes and carboxylic acids via metal/bromide catalysts in acetic acid/water mixtures. *Adv Synth Catal* . 2009;351(3):456-466.
46. Voitl T, Rohr PRV. Oxidation of lignin using aqueous polyoxometalates in the presence of alcohols. *ChemSusChem* . 2008;1:763-769.

Hosted file

Tables.docx available at <https://authorea.com/users/325431/articles/453415-oxidation-of-organosolv-lignin-in-a-novel-surfactant-free-microemulsion-reactor>

